

# **Closely piling up of multiple adhesive fronts in adhesive friction due to re-attachment**

Puyu Cao<sup>1</sup>, Meicheng Yao<sup>1</sup>, Bin Chen<sup>1,2\*</sup>

<sup>1</sup>Department of Engineering Mechanics, Zhejiang University, Hangzhou, China

<sup>2</sup>Key Laboratory of Soft Machines and Smart Devices of Zhejiang Province, Hangzhou,  
China

\* To whom correspondence should be addressed: chenb6@zju.edu.cn

## **Abstract**

Friction impacts a wide range of fields, spanning engineering, geology, biomechanics, and numerous others. As a fundamental force, it influences various aspects of our daily lives and industrial processes across multiple disciplines. To understand how adhesive friction seemingly breaks the size limit dictated by the fracture theory, here we investigate the sliding of elastic solids adhered to a rigid surface via multiple adhesive springs. With the consideration of random re-attachment of detached adhesive springs, we find that the shear-off force of the interface can significantly exceed predictions made by the fracture theory, with substantial adhesive forces distributed across the entire interface. Through this observation, we identify multiple adhesive fronts closely aligning along the interface, exhibiting similar force profiles. Moreover, the number of these regions seems to generally increase with the interface size, resulting in a linear rise in the calculated shear-off force with interface

size. Therefore, we conclude that the close accumulation of multiple adhesive fronts along an interface aids each other through random healing so as to erase the size effect of the fracture theory, which offers valuable insights into understanding the phenomena associated with adhesive friction along an interface in various fields.

## **Introduction**

Friction is an essential phenomenon that affects our daily lives and various industrial processes<sup>1</sup>. At macroscopic scales, friction typically follows Amonton's law<sup>2</sup> across the majority of dry or lubricated interfaces<sup>3-5</sup>, where it varies directly with the applied normal force. However, at microscopic or molecular levels, Bowden and Tabor<sup>6</sup> suggested that friction is associated with the real contact area between weakly adhering surfaces, which can often be significantly smaller than the apparent contact area. The proposition by Bowden and Tabor<sup>6</sup> would align with Amonton's law if the real contact area is roughly proportional to the applied normal load<sup>4</sup>. While experimental evidence supports the proposition by Bowden and Tabor<sup>6</sup>, showing that the frictional force correlates with the real contact area for both multi-contacts<sup>7-13</sup> and single contacts<sup>6,14,15</sup> between smooth bodies, with the proportionality constant being the frictional shear strength of the contact, this proposition appears to challenge the fracture theory.

As one main type of friction between two dry surfaces, adhesive friction arises when adhesive bonds form within the contacting junctions due to molecular or atomic interactions<sup>1</sup>. Considering that two surfaces adhere through adhesive bonds, the adhesive force would typically concentrate heavily at a single adhesive front, usually

with the size of the cohesive zone, as explained by the fracture theory<sup>16</sup>. As individual asperities reach nanoscale sizes, the flaw tolerance effect<sup>17,18</sup> occurs, wherein the strength criteria<sup>19</sup>, rather than the energy criteria<sup>16</sup>, govern the behavior of fracture. By disregarding the elastic interaction between neighboring asperities at the microscale, as commonly done in existing theories, the flaw tolerance theory<sup>17,18</sup> may explain the observation that the frictional force correlates with the real contact area for both multi-contacts<sup>7-13</sup> and single contacts<sup>6,14,15</sup> between smooth bodies, with the proportionality constant being the frictional shear strength of the contact.

Unfortunately, as showed in our previous research based on the fracture theory, it is essential not to overlook the elastic interactions among neighboring contact junctions<sup>20,21</sup>. When there is a periodic distribution of cohesive energy along an interface due to defects, the apparent fracture energy of the interface should lie within the range defined by the peak value and the average value of the cohesive energy<sup>21</sup>. Indeed, it has been demonstrated that only specific hierarchical structures with multiscale features can efficiently aggregate adhesive forces collected at multiple adhesive units of small scales<sup>22</sup>. The mystery of why the frictional force remains proportional to the real contact area persists from our perspective.

Localized healing of broken parts along the interface can play a crucial role in friction<sup>23</sup>. Here, by considering the random re-attachment/healing of broken adhesive elements, we investigate the adhesive friction when sliding elastic solids across a rigid surface that adhere to each other through multiple adhesive springs. Intriguingly, our analysis reveals that the calculated friction can significantly surpass the predictions of

the fracture theory. By studying the distribution of adhesive force along the interface, we observe substantial adhesive forces acting across the entire interface. We also identify multiple adhesive fronts accumulating along the interface, exhibiting similar force profiles. The number of these regions generally increases with the size of the interface. These adhesive fronts appear to support each other, leading to a linear growth in the calculated shear-off force with the contact area, which apparently breaks the size limit dictated by the fracture theory. This work provides valuable insights into comprehending the observed behavior concerning adhesive friction in various fields.

### **Adhesive friction of relatively thin elastic solids**

We firstly investigate relatively thin elastic solids sliding on a rigid surface with  $H/d = 10$  and simulation results are displayed in Fig. 1. Without re-attachment of detached adhesive elements, i.e.,  $k_{on}^0 = 0\text{s}^{-1}$ , we observe four distinct phases in the evolution of the frictional force, denoted as  $F$ . In Phase 1, the frictional force steadily increases, reaching a peak value in Phase 2, followed by a decrease to zero in Phase 3, and eventually maintaining at zero in Phase 4. The real contact area, denoted as  $A$ , is calculated by multiplying the number of attached adhesive springs by  $d$  and unit width, which gradually diminishes to zero within a relatively short shear displacement in Fig. 1b. The prediction from the Kendall model<sup>24</sup> for the frictional force in Phase 2, denoted as  $F_{0T}$ , is given by  $f_b \sqrt{\frac{EH}{kd}}$ , which yields a value of 130 pN, aligning closely with the peak value of 140 pN obtained in our numerical simulation.

For non-zero but relatively small  $k_{on}^0$ , Fig. 1a shows notable differences arising

in Phase 2 and Phase 4. In Phase 2, the frictional force exhibits an increase with shear displacement that surpasses the prediction of Kendall's theory<sup>24</sup>. In Phase 4, the frictional force is no longer zero and exhibits fluctuation, which closely resemble the stick-slip phenomenon, where it generally increases during the "stick" phase and subsequently abruptly decreases during the "slip" phase. Notably, the peak frictional force in Phase 4, denoted as  $F_p$ , is significantly lower than that in Phase 2. Figure 1b reveals that a small portion of adhesive springs attach to the substrate with its number fluctuating in Phase 4. As  $k_{on}^0$  increases, the peak frictional force both in Phase 2 and Phase 4 increases. With further increase in  $k_{on}^0$ , Phase 2 becomes indistinguishable and the frictional force in Phase 4 displays significant fluctuations. Importantly, during these fluctuations, the peak frictional force can exceed by a large margin the prediction provided by the classical Kendall model. For instance, when  $k_{on}^0 d/V = 0.6$ , the former can surpass the latter by more than 200%. In Fig. 1b, it is evident that a large portion of springs attach to the substrate, although their number fluctuates. When plotting out the largest peak frictional force in Phase 4, denoted as  $F_s$ , against  $k_{on}^0$  in Fig. 1c, we find that it generally increases with  $k_{on}^0$  until it saturates at a large  $k_{on}^0$ .

To see how the peak frictional force in Phase 4 with large  $k_{on}^0$  can be even much larger than the prediction made by the classical Kendall's model<sup>24</sup>, we plot out representative adhesive forces along the interface in Extended Data Figure 1. When  $k_{on}^0 = 0$ , only a single region of crack-like force profile, i.e., the adhesive front, is observed along the interface, where only a small number of adhesive springs are strained, while the remaining adhesive springs exert no force. In contrast, with a large

$k_{on}^0$  value, such as  $k_{on}^0 d/V = 0.6$ , two regions of crack-like force profiles, i.e., two adhesive fronts, may emerge in close proximity along the interface, as shown in Extended Data Figure 1b. Consequently, a significant portion of adhesive springs would experience strain along the interface, resulting in a much higher frictional force than predicted by Kendall's model, despite non-uniform forces within the adhesive springs.

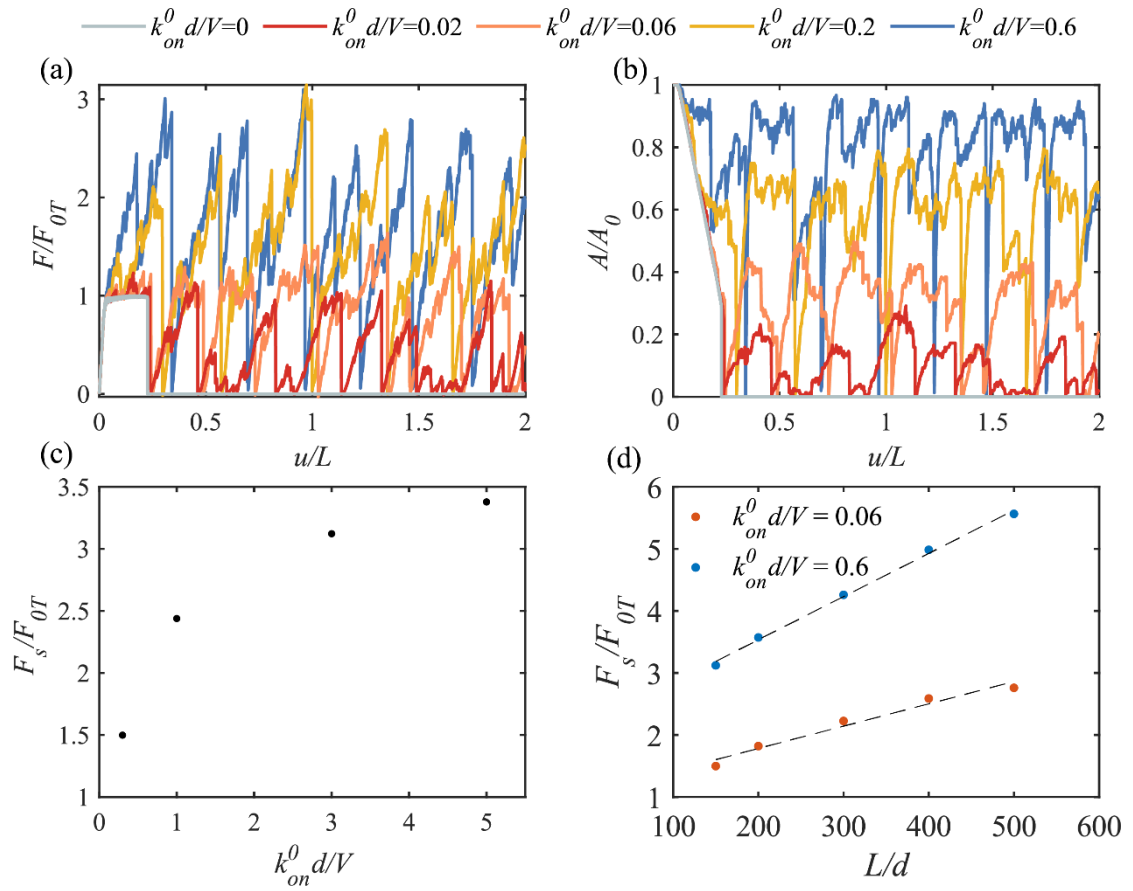


**Fig. 1.** Simulation results for relatively thin elastic solids: Variation of the frictional force (a) and the contact area (b) with the sliding displacement at different  $k_{on}^0$ ; (c) Effect of  $k_{on}^0$  on the peak frictional force in Phase 4. (d) The variation of the shear off force with  $L$ . In the analysis,  $H = 10d$ .

The adhesive friction was observed to exhibit a linear relationship with the real contact area in experimental studies<sup>25,26</sup>. To see if our model can generate comparable predictions, we adjust the length of the elastic solids in our simulations, which represents the size of the interface. In the analysis, we calculate the average of the peak forces in Phase 4, termed as the shear-off force, denoted as  $F_S$ . In Fig. 1d, we observe that  $F_S$  appears to linearly increase with  $L$ . To gain further insight, we plot particular adhesive forces along the interface at certain displacements in Figs. 2a-f. These figures reveal that the number of adhesive fronts generally increases with  $L$ . It appears that the adhesive frictional forces generated within these adhesive fronts effectively support each other, leading to a linear increase in the shear off force as the size of the interface increases. The slope of a linear fitting curve in Fig. 1d would correspond to  $\frac{\Delta F/F_{0T}}{\Delta L/d}$ , which is found to be 0.0073 for  $k_{on}^0 d/V = 0.6$ . If the friction force generated within each adhesive front is assumed to be  $F_{0T}$ , the size of each adhesive front equal and no gap exist between neighboring adhesive fronts for  $k_{on}^0 d/V = 0.6$ , then  $\frac{\Delta L}{\Delta F/F_{0T}}$  would be size of each adhesive front. In this way, the size of each adhesive front is estimated to be  $137d$ , which is close to the simulated size of the single adhesive front without reattachment displayed in Extended Data Figure 1. Comparing Figs. 2a-c with Figs. 2d-f, it can also be observed that a lower reattachment rate can not only result in a reduced density of adhesive fronts along the interface but also decrease the frictional force induced within individual adhesive fronts. Note that Fig. 2 also indicates that adhesive defects would be generally generated even on an initially perfectly adhered interface in adhesive friction.

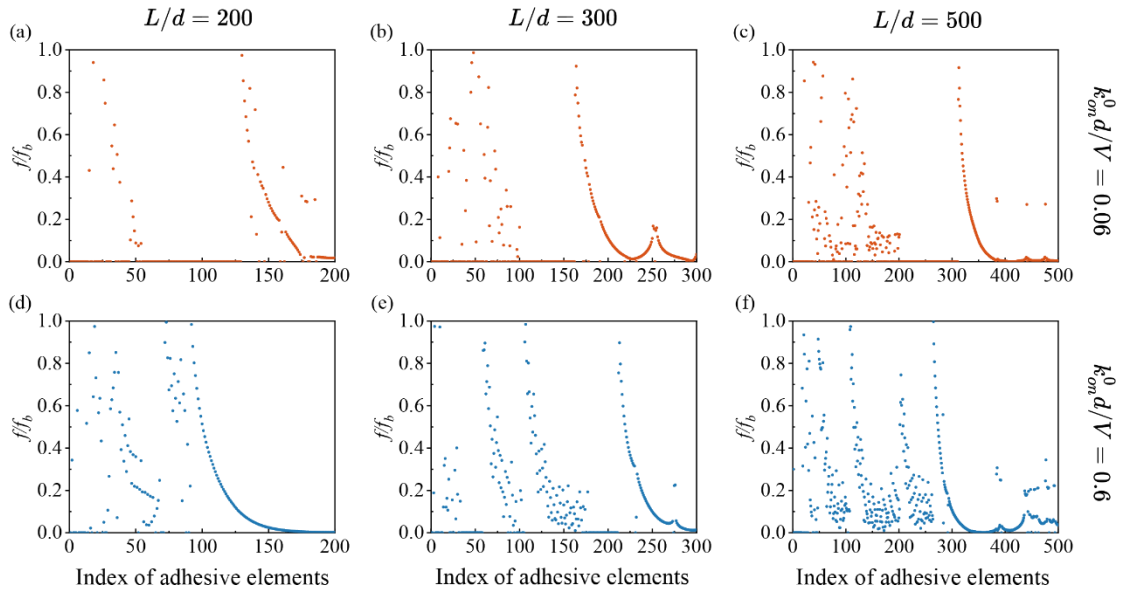


**Fig. 2.** Effects of  $L$  of relatively thin elastic solids on the adhesive friction: The particular distribution of adhesive forces along the interface at certain sliding displacements for different  $L$  when  $k_{on}^0 d/V = 0.06$  (a-c) or  $k_{on}^0 d/V = 0.6$  (d-f). In the analysis,  $H = 10d$ .

### Adhesive friction of relatively thick elastic solids

In order to explore the generality of these findings regarding adhesive friction in relatively thin elastic solids, we furtherly investigate relatively thick elastic solids with  $H/d = 300$ . The frictional force during Phase 2, denoted as  $F_{0B}$ , slightly varies in Fig. 3a when  $k_{on}^0 = 0$ , due to the resulting minor bending along the interface. In Extended Data Figure 2, only a single adhesive front exists along the interface when  $k_{on}^0 = 0$ . For non-zero  $k_{on}^0$ , the frictional force in Phase 4 displays the stick-slip phenomenon. In Fig. 3c, the peak frictional force,  $F_p$ , in Phase 4 shows a rising trend with  $k_{on}^0$  until it reaches a saturation point at large  $k_{on}^0$ , which can be notably higher than the case

without re-attachment. Additionally, in Extended Data Figure 2, it can be observed that a significant proportion of adhesive springs along the interface experience strain for large values of  $k_{on}^0$ . When varying the size of the interface,  $L$ , in our simulation, we find that the shear-off force exhibits a linear relationship with  $L$  in Fig. 3d. Figures. 4a-f and also Extended Data Figure 3 reveal that the number of adhesive fronts generally increases with  $L$ , which is much clearer for higher  $k_{on}^0 d/V$ , and the separation between neighboring adhesive fronts can be smaller than the size of an adhesive front. With the slope of a linear fitting curve for  $k_{on}^0 d/V = 0.6$  being 0.0037, the size of an adhesive front is estimated to be  $270d$ , close to the simulated size of the single adhesive front without re-attachment displayed in Extended Data Figure 2. These findings on relatively thick elastic solids align closely with the observations made in relatively thin elastic solids, indicating their general applicability to elastic solids.

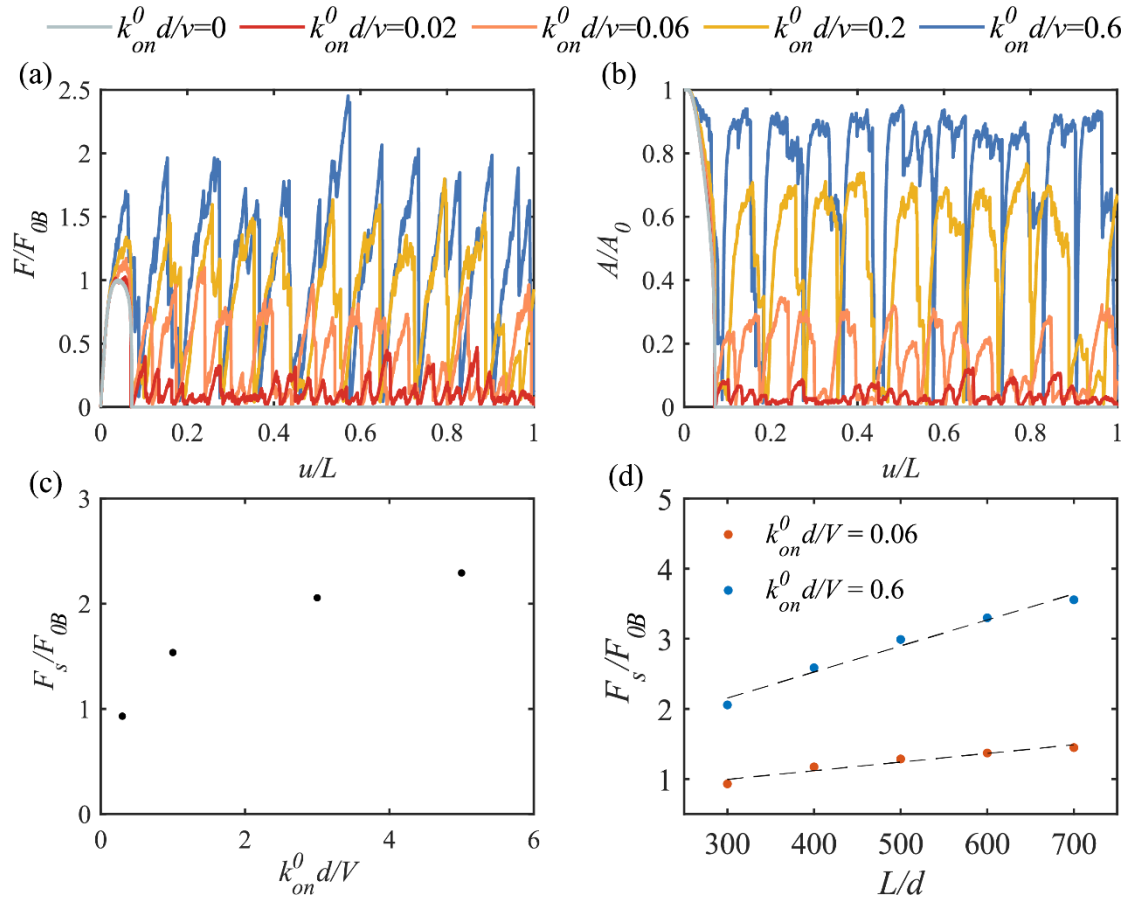


**Fig. 3.** Simulations results for relatively thick elastic solids: Variation of the frictional force (a) and the contact area (b) with the sliding displacement at different  $k_{on}^0$ ; (c) Effect of  $k_{on}^0$  on the peak value of the frictional force in Phase 4; (d) The variation of the shear off force with  $L$ . In the analysis,  $L = 300d$  for (a-c) and  $H = 100d$ .

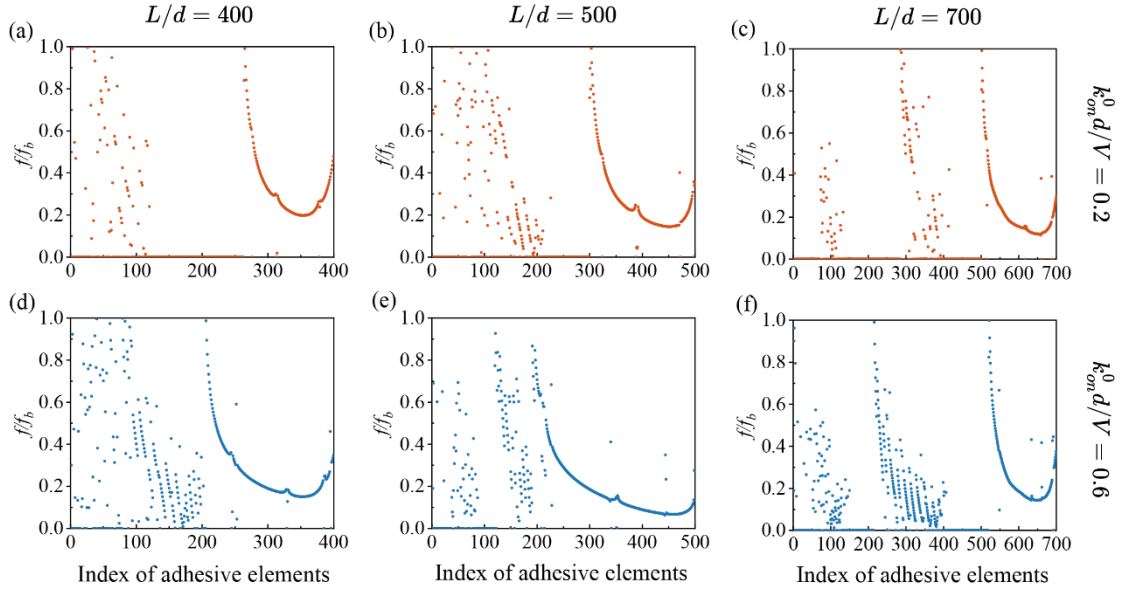


**Fig. 4.** Effect of  $L$  of relatively thick elastic solids on the adhesive friction: The particular distribution of adhesive forces along the interface at certain sliding displacements for different  $L$  when  $k_{on}^0 d/V = 0.2$  (a-c) or  $k_{on}^0 d/V = 0.6$  (d-f). In the analysis,  $H = 100d$ .

### Effect of adhesive defects

We also investigate the effect of adhesive defects that commonly present along rough interfaces. Without re-attachment/healing of detached adhesive elements, our analysis shows that there would still exist only a single adhesive front along the interface and the frictional force for the interface with adhesive defects would not be over that without defects in Extended Data Figure 4, consistent with our previous findings<sup>21</sup>. However, with random healing of detached adhesive elements, our further analysis indicates that there would exist multiple regions of adhesive fronts backing up each other along the interface with adhesive defects, leading to a much higher adhesive frictional force, which is consistent with results above.

## **Effect of sliding velocities**

It is widely believed that slower sliding velocities would provide more time for contact areas to expand, accounting for the common observation that kinetic friction typically increases as sliding velocity decreases. In accordance with our analysis, lower sliding velocities would be equivalent to higher re-attachment/healing rates, upon which a larger number of adhesive elements can heal after detachment. In this way, slower sliding velocities would induce higher adhesive frictional forces along an interface, as demonstrated in our analysis shown in Fig. 5a. However, our analysis also indicates that contact area alone cannot fully elucidate the variations in adhesive frictional forces at different sliding velocities. Crucially, due to the healing of detached adhesive elements, adhesive forces along the interface are also redistributed, leading to the buildup of multiple adhesive fronts that significantly impact adhesive frictional force along the interface as sliding velocity changes.

## **A general law of the adhesive friction**

Our analysis indicates that the backing up of multiple adhesive fronts in adhesive friction, facilitated by random re-attachment/healing, contributes to the linear growth in the adhesive frictional force with interface size, significantly aligning with experimental findings<sup>7-14</sup> and apparently breaking the size limit dictated by the classical fracture theory<sup>16</sup>. Based on these results, we suggest a general law of the adhesive friction that the shear-off force of an adhesive interface can be given by  $F_s = \rho F_A A_0$ , where  $\rho$  is the average area density of the adhesive fronts piling up along the interface,

$F_A$  the average frictional force generated within a single adhesive front, both of which are expected to depend on the re-attachment/healing rate and the sliding velocities, and  $A_0$  the initial contact area. It is important to emphasize that, in the current work, the interface size corresponds to the real contact area at rest, which differs from the real contact area in motion. The latter continues to evolve during sliding, as revealed in our analysis.

## **Discussions**

In our analysis, the stick-slip phenomenon arises along the interface due to re-attachment/healing of detached adhesive elements. A significant amount of elastic energy is accumulated within the stick phase, which will be released during the slip phase. Such a dynamic behavior might give rise to various issues in noise generation, earthquakes, etc. Consistently, as observed in earthquake rupture, the self-healing pulse of slips<sup>27</sup> was suggested to lead to a large radiated energy of earthquakes<sup>28</sup>.

As seen from the typical evolution of adhesive forces along the interface displayed in Extended Data Figure 5, small incremental slips occur during both the stick phase and the slip phase in the frictional adhesion. Such incremental slips were observed in experiments of peeling adhesive tapes<sup>29</sup> or shearing of two blocks along a frictional interface<sup>23</sup>. Extended Data Figure 5 indicates that these small incremental slips can be due to the breaking of individual adhesive bonds, a single adhesive front, or a bunch of adhesive fronts, etc., which are apparently of different time scales and size scales. Extended Data Figure 5 clearly shows how discrete tiny adhesive sites along the

interface can grow into relatively large adhesive fronts and sequentially pile up accompany these incremental slips. These insights derived from our model analysis might help elucidate the connections between after slips detected via geodetic techniques and aftershocks captured by seismic surveillance, and also pave the way for advanced methods in earthquake prediction.

Pretension<sup>20</sup> was utilized to explain the force-independent critical detachment angle observed in Gecko adhesion<sup>30-32</sup>. Nevertheless, one might raise concerns regarding the stringent requirements needed to actively generate a high level of pretension within a spatula pad through sequential attachment<sup>20</sup>. As suggested by Figs. 2-3, the random re-attachment/healing of broken adhesive elements at a high healing rate can effectively induce substantial pretension within an elastic solid, which shares significant similarities with the behavior of a spatula pad interacting with surfaces through van der Waals forces, where a high re-attachment/healing rate might be expected. Thus, our current analysis suggests that the establishment of high pretension within a spatula pad is indeed achievable and can be robust.

If a single adhesive spring in our model analysis physically corresponds to a single molecular interaction, its bond breaking can also be random and controlled by force. The bond breaking rate, denoted as  $k_{off}$ , can be, for example, described by the Bell's law<sup>33</sup>, given by  $k_{off} = k_{off}^0 \exp\left(\frac{f}{f_b}\right)$ , with  $k_{off}^0$  being the bond breaking force without force and  $f_b$  being a force scale. We also simulate the case with such force-controlled random breaking of adhesive springs, as often studied in cell mechanics<sup>34</sup>. Our simulations in Fig. 5b indicates that the adhesive frictional force still appears to be

stick and slip and the adhesive frictional force of softer solids can be higher than that of stiffer solids, depending on both the re-attachment rate and the breaking rate. The shear-off force still linearly increases with the size of the interface in Fig. 5c. Most importantly, as we plot out adhesive forces along the interface, we also observe substantial adhesive forces along the entire interface in Fig. 5d, which are similar as found above.

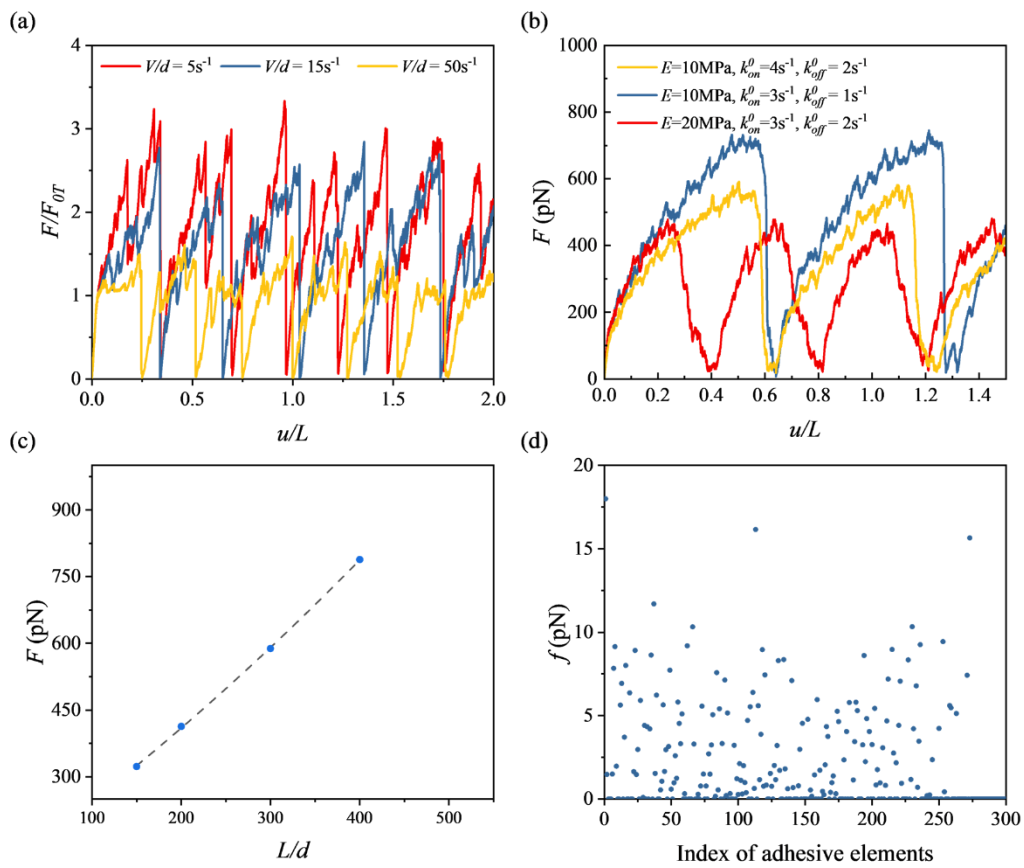


**Fig. 5.** (a) Effect of the sliding velocity on the frictional force; (b-d) When the breaking of adhesive springs becomes randomly force-dependent, the adhesive frictional force of softer solids can be higher than that of stiffer solids, depending on both the re-attachment rate and the breaking rate (b), the shear off force linearly increases with the size of interface (c), and substantial adhesive forces can exist along the entire interface.

In the analysis for (c-d),  $k_{on}^0 = 3s^{-1}$  and  $k_{off}^0 = 1s^{-1}$ .

## Conclusion

Our analysis focuses on studying the adhesive friction force along an interface. We find that the calculated friction force can exceed the predictions of fracture theory. Through our analysis, we have identified multiple adhesive fronts that closely pile up along the interface. These regions can exhibit similar force profiles, and their quantity appears to increase with the size of the interface. Consequently, this increase leads to a linear growth in the calculated shear-off force with the size of the interface, which apparently breaks the size limit dictated by the classical fracture theory. We believe that these findings provide deep insights into understanding the abundant phenomena associated with adhesive friction along an interface in various fields.

## References:

1. Mate, C. M. & Carpick, R. W. Tribology on the small scale: A bottom up approach to friction, lubrication, and wear. *J. Phys. Math. Theor.* **41**, 479002 (2019).
2. Blau, P. J. Amontons' laws of friction. in *Encyclopedia of Tribology* (eds. Wang, Q. J. & Chung, Y.-W.) 71–71 (Springer US, Boston, MA, 2013). doi:10.1007/978-0-387-92897-5\_166.
3. Berman, A., Drummond, C. & Israelachvili, J. Amontons' law at the molecular level. *Tribol. Lett.* **4**, 95–101 (1998).
4. *Physics of Sliding Friction*. (Springer Netherlands, Dordrecht, 1996). doi:10.1007/978-94-015-8705-1.

5. Rabinowicz, E. & Tanner, R. I. Friction and wear of materials. *J. Appl. Mech.* **33**, 479–479 (1966).
6. Bowden, F. P. & Tabor, D. *The Friction and Lubrication of Solids*. vol. 1 (Oxford university press, 2001).
7. Elastic deformation and the laws of friction. *Proc. R. Soc. Lond. Ser. Math. Phys. Sci.* **243**, 190–205 (1957).
8. Dieterich, J. H. & Kilgore, B. D. Direct observation of frictional contacts: New insights for state-dependent properties. *Pure Appl. Geophys. PAGEOPH* **143**, 283–302 (1994).
9. Rubinstein, S. M., Cohen, G. & Fineberg, J. Detachment fronts and the onset of dynamic friction. *Nature* **430**, 1005–1009 (2004).
10. Yashima, S. *et al.* Normal contact and friction of rubber with model randomly rough surfaces. *Soft Matter* **11**, 871–881 (2015).
11. Degrandi-Contraires, E., Poulard, C., Restagno, F. & Léger, L. Sliding friction at soft micropatterned elastomer interfaces. *Faraday Discuss.* **156**, 255 (2012).
12. Okamoto, Y., Nishio, K., Sugiura, J., Hirano, M. & Nitta, T. Friction of elastomer-on-glass system and direct observation of its frictional interface. *J. Phys. Conf. Ser.* **89**, 012011 (2007).
13. Wu-Bavouzet, F., Cayer-Barrioz, J., Le Bot, A., Brochard-Wyart, F. & Buguin, A. Effect of surface pattern on the adhesive friction of elastomers. *Phys. Rev. E* **82**, 031806 (2010).
14. Carpick, R. W. & Salmeron, M. Scratching the surface: Fundamental investigations

- of tribology with atomic force microscopy. *Chem. Rev.* **97**, 1163–1194 (1997).
15. Cohen, C., Restagno, F., Poulard, C. & Léger, L. Incidence of the molecular organization on friction at soft polymer interfaces. *Soft Matter* **7**, 8535 (2011).
  16. Gdoutos, E. E. *Fracture Mechanics: An Introduction*. vol. 263 (Springer International Publishing, Cham, 2020).
  17. Gao, H., Ji, B., Buehler, M. J. & Yao, H. Flaw tolerant bulk and surface nanostructures of biological systems. *Mech. Chem. Biosyst. MCB* **1**, 37–52 (2004).
  18. Gao, H., Ji, B., Jäger, I. L., Arzt, E. & Fratzl, P. Materials become insensitive to flaws at nanoscale: Lessons from nature. *Proc. Natl. Acad. Sci.* **100**, 5597–5600 (2003).
  19. Gere, J. M. & Timoshenko, S. P. *Mechanics of Materials*. (Stanley Thornes, 1999).
  20. Chen, B., Wu, P. & Gao, H. Pre-tension generates strongly reversible adhesion of a spatula pad on substrate. *J. R. Soc. Interface* **6**, 529–537 (2009).
  21. Chen, B., Shi, X. & Gao, H. Apparent fracture/adhesion energy of interfaces with periodic cohesive interactions. *Proc. R. Soc. Math. Phys. Eng. Sci.* **464**, 657–671 (2008).
  22. Chen, B., Wu, P. D. & Gao, H. Hierarchical modelling of attachment and detachment mechanisms of gecko toe adhesion. *Proc. R. Soc. Math. Phys. Eng. Sci.* **464**, 1639–1652 (2008).
  23. Shi, S., Wang, M., Poles, Y. & Fineberg, J. How frictional slip evolves. *Nat. Commun.* **14**, 8291 (2023).
  24. Kendall, K. Thin-film peeling—the elastic term. *J. Phys. Appl. Phys.* **8**, 1449–1452

- (1975).
25. Yoon, E.-S., Singh, R. A., Oh, H.-J. & Kong, H. The effect of contact area on nano/micro-scale friction. *Wear* **259**, 1424–1431 (2005).
  26. Enachescu, M. *et al.* Observation of proportionality between friction and contact area at the nanometer scale. *Tribol. Lett.* **7**, 73–78 (1999).
  27. Heaton, T. H. Evidence for and implications of self-healing pulses of slip in earthquake rupture. *Phys. Earth Planet. Inter.* **64**, 1–20 (1990).
  28. Lambert, V., Lapusta, N. & Perry, S. Propagation of large earthquakes as self-healing pulses or mild cracks. *Nature* **591**, 252–258 (2021).
  29. Dalbe, M.-J., Cortet, P.-P., Ciccotti, M., Vanel, L. & Santucci, S. Multiscale stick-slip dynamics of adhesive tape peeling. *Phys. Rev. Lett.* **115**, 128301 (2015).
  30. Autumn, K. *et al.* Adhesive force of a single gecko foot-hair. *Nature* **405**, 681–685 (2000).
  31. Autumn, K. *et al.* Evidence for van der Waals adhesion in gecko setae. *Proc. Natl. Acad. Sci.* **99**, 12252–12256 (2002).
  32. Autumn, K., Dittmore, A., Santos, D., Spenko, M. & Cutkosky, M. Frictional adhesion: A new angle on gecko attachment. *J. Exp. Biol.* **209**, 3569–3579 (2006).
  33. Bell, G. I. Models for the specific adhesion of cells to cells: A theoretical framework for adhesion mediated by reversible bonds between cell surface molecules. *Science* **200**, 618–627 (1978).
  34. Chen, B., Ji, B. & Gao, H. Modeling active mechanosensing in cell-matrix interactions. *Annu. Rev. Biophys.* **44**, 1–32 (2015).

35. Kramers, H. A. Brownian motion in a field of force and the diffusion model of chemical reactions. *Physica* 7, 284–304 (1940).

## Methods

We examine a scenario where a generic 2-D elastic solid with unit thickness adheres to a smooth rigid surface through multiple adhesive elements distributed along the interface, as illustrated in Fig. 6. Each adhesive element may represent an individual molecular interaction, a cluster of interactions, or even a single asperity. Though sophisticated adhesive elements were developed in the literature, we simplify each adhesive element as a linear spring in our analysis without losing its generality.

The elastic solid has a length of  $L$  and a height of  $H$ . It has an elastic modulus of  $E$  and a Poisson's ratio of  $\nu$ . Adhesive springs with a spring constant of  $k$  are uniformly distributed along the bottom surface of the elastic solid with a spacing of  $d$ , which are numbered sequentially from the left to the right. Adhesive sites along the rigid surface are also uniformly distributed with the same spacing of  $d$ . The elastic solid is subjected to a horizontal sliding toward the right at a velocity of  $V$ .

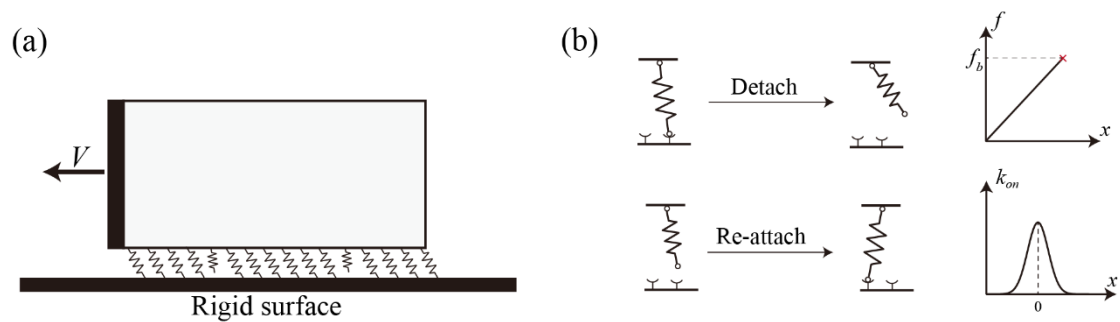


**Fig. 6.** (a) A generic mechanics model comprises of an elastic solid, adhering to a rigid

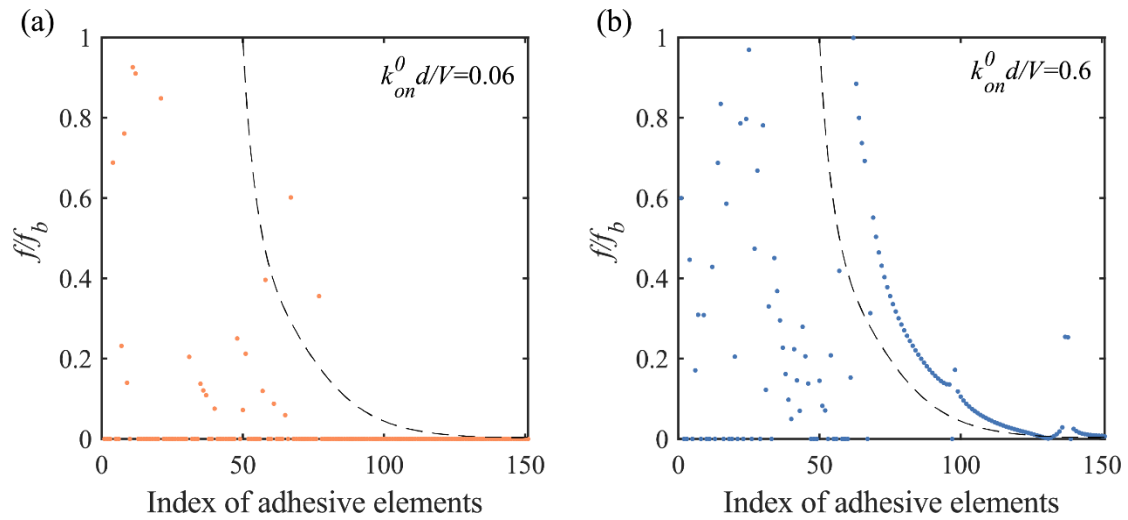
surface through multiple adhesive elements uniformly distributed along the interface. Without losing generality, each adhesive element is simplified as a linear spring. The elastic solid is subjected to a horizontal sliding to the right with a velocity  $V$ . (b) In the model, an attached spring would deterministically detach at a critical force,  $f_b$ , and a detached spring can randomly re-attach to the interface to heal with a rate of  $k_{on}$  guided by the elastic energy, both of which depend on the spring extension,  $x$ .

Initially, all adhesive springs attach to adhesive sites on the rigid surface with zero extension. The initial contact area, denoted as  $A_0$ , is given by  $L$  times the unit width of a 2-D structure. When the elastic solid is pulled, these springs would be stretched. A spring is assumed to detach from its adhesive site on the substrate once the force within it reaches the adhesive strength of  $f_b$ . Detached springs are allowed to randomly re-attach to an open adhesive site to heal on the rigid surface at a rate of  $k_{on}$ , which is guided by the elastic energy. Without losing its generality,  $k_{on}$  is assumed to follow the Kramer's law<sup>35</sup>, given by  $k_{on} = k_{on}^0 \cdot e^{-\frac{\Delta U}{k_B T}}$ , where  $\Delta U$  is the elastic energy that would be stored within the spring upon its potential attachment,  $k_{on}^0$  is the attachment rate when  $\Delta U = 0$ ,  $k_B$  is the Boltzmann constant, and  $T$  is the absolute temperature. As the elastic solid slides, adhesive springs along the interface continue to detach and randomly re-attach to the rigid surface and the reaction force would be induced at the sliding end of the elastic solid, which would be taken as the adhesive frictional force.

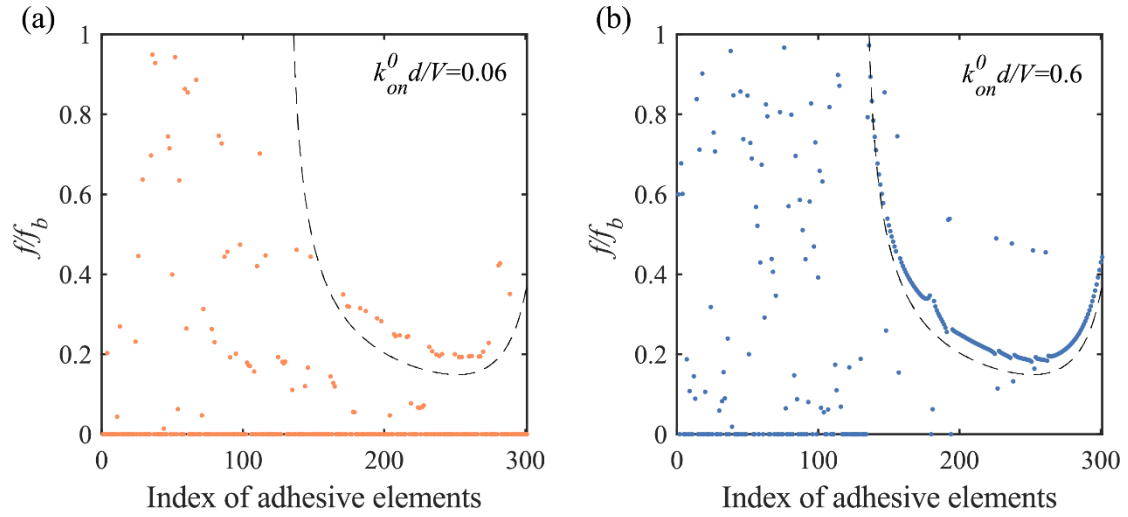
The model is simulated with the coupled Finite Element Analysis and the Monte Carlo method. Within this numerical scheme, the deformation and the force within the

model are calculated with Finite Element Analysis at each time step. If the force within an adhesive spring, denoted as  $f$ , reaches  $f_b$ , the spring would detach from the rigid surface. Otherwise, the Monte Carlo method will be employed to determine where and when a detached adhesive spring would randomly re-attach/heal to the rigid surface at the next time step. Default values of parameters used in the simulations are provided in Extended Data Table 1. To calculate the average of the peak force in Phase 4, termed as the shear-off force, we run simulations of pulling relatively thin and thick elastic solids for 100 trajectories and also ensure the occurrence of at least one stick-slip event within each trajectory.

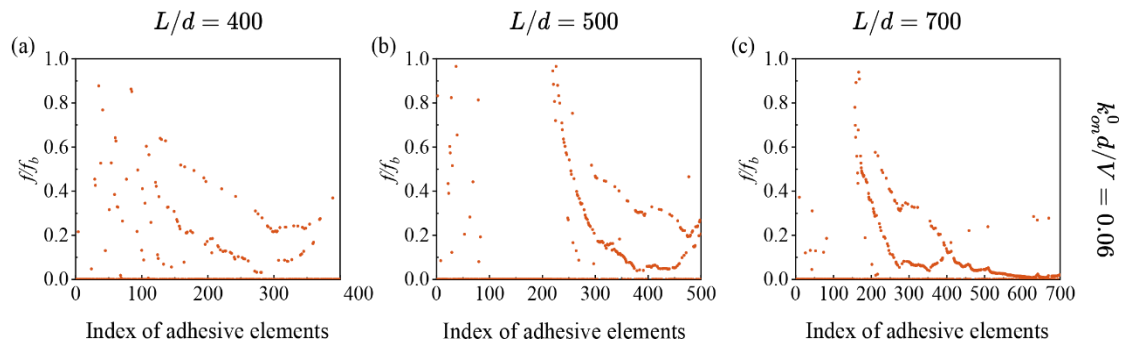
## Extended Data



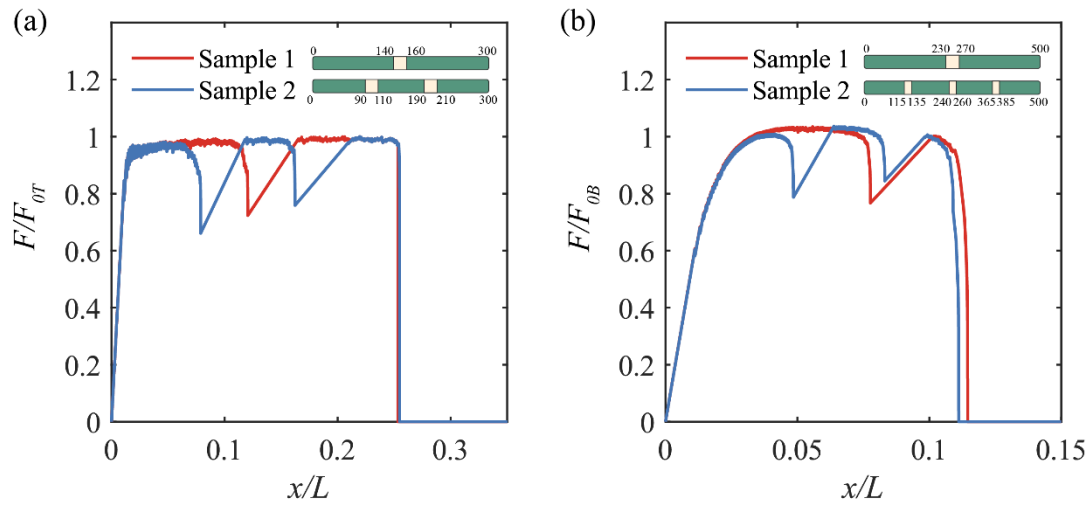
**Extended Data Figure 1.** The distribution of adhesive forces of relatively thin elastic solids along the interface at  $u/L = 1.4$  when  $k_{on}^0 d/V = 0.06$  (a) and  $k_{on}^0 d/V = 0.6$  (b), where the dashed line represents the adhesive force distribution without re-attachment/healing. In the analysis,  $H = 10d$ .



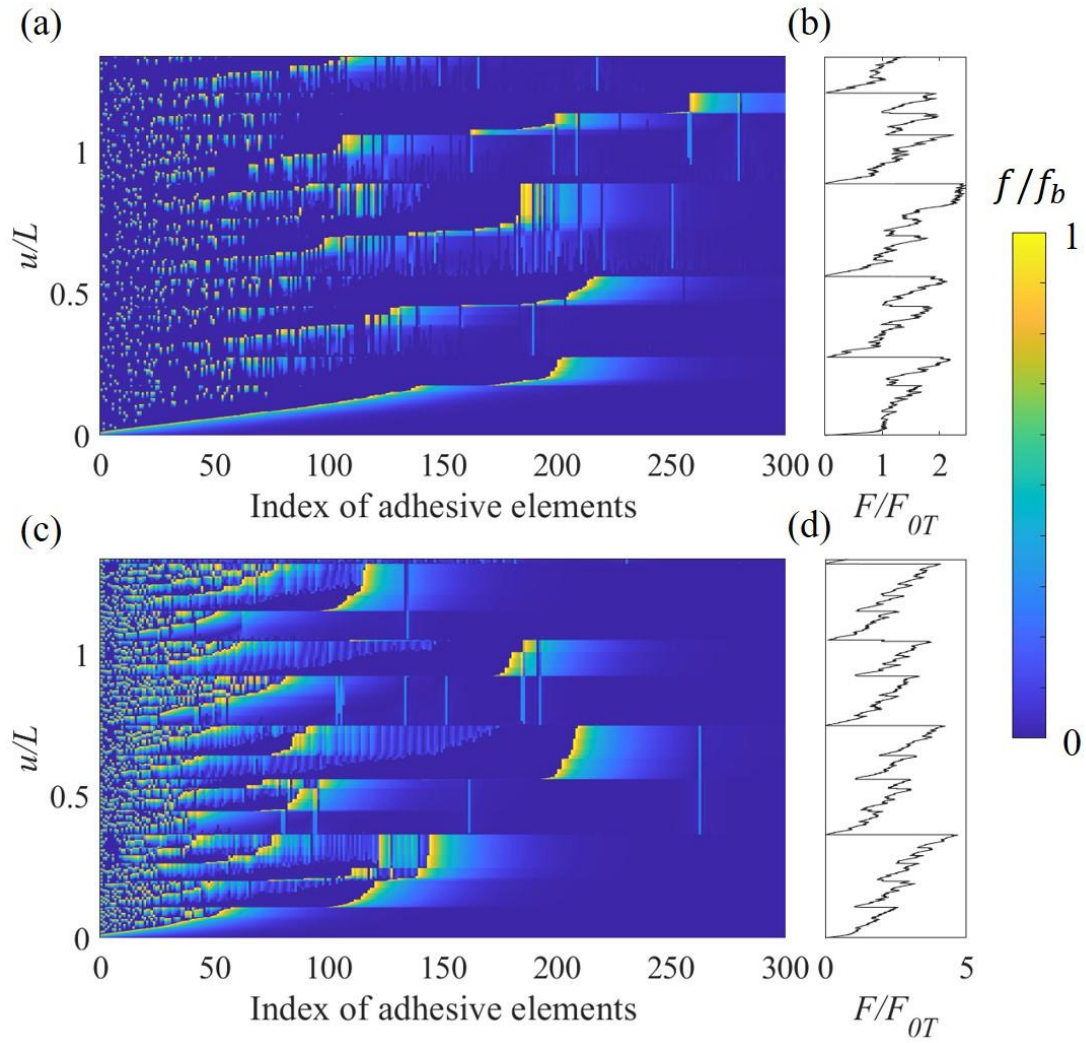
**Extended Data Figure 2.** The distribution of adhesive forces of relatively thick elastic solids along the interface at  $u/L = 0.2667$  when  $k_{on}^0 d/V = 0.06$  (a) and  $k_{on}^0 d/V = 0.6$  (b), where the dash line represents the adhesive force distribution without re-attachment/healing. In the analysis,  $H = 100d$ .



**Extended Data Figure 3.** Effect of  $L$  of relatively thick elastic solids on the adhesive friction: The particular distribution of adhesive forces along the interface at certain sliding displacements for different  $L$  when  $k_{on}^0 d/V = 0.06$ . In the analysis,  $H = 100d$ .



**Extended Data Figure 4.** Effect of adhesive defects along the interface on the frictional force of relatively thin elastic solids with  $L = 300d$  and  $H = 10d$  (a) or relatively thick elastic solids with  $L = 500d$  and  $H = 100d$  (b) on a rigid surface without re-attachment/healing. Missing adhesive springs along the interface for different samples are indicated with blank space in insets.



**Extended Data Figure 5.** Contour plots show typical evolution of adhesive forces along the interface in adhesive friction with low re-attachment rate ( $k_{on}^0 d/V = 0.06$ ) (a) and with high re-attachment rate ( $k_{on}^0 d/V = 0.6$ ) (c) together with respective evolution of corresponding frictional forces (b, d). In the simulation,  $L = 300d$ .

**Extended Data Table 1** Default values of parameters in the simulations

Parameter	Value	Parameter	Value
$L$	1500 nm	$k$	0.3 pN/nm
$H$	100 nm	$k_{on}^0$	$3 \text{ s}^{-1}$
$E$	5 MPa	$d$	10 nm
$v$	0.3	$V$	50 nm/s
$f_b$	10 pN	$k_B T$	4.14 pN.nm

## **Acknowledgements**

This work was supported by the National Natural Science Foundation of China (Grant No.: 12372318, 11872334), and Zhejiang Provincial Natural Science Foundation of China (Grant No.: LZ23A020004).

**Author contributions:** B.C. designed research, P.C. and B.C. performed research, P.C. and M.Y. analyzed data, P.C. and B.C. wrote the manuscript.

**Competing Interest Statement:** The authors declare no competing interests.

Correspondence and requests for materials should be addressed to [chenb6@zju.edu.cn](mailto:chenb6@zju.edu.cn)